Observing stochastic resonance in an underdamped bistable Duffing oscillator by the method of moments

Yan-Mei Kang,* Jian-Xue Xu,† and Yong Xie‡
Institute for Nonlinear Dynamics, School of Architectural Engineering and Mechanics, Xi'an Jiaotong University, Xi'an 710049, China
(Received 27 November 2002; revised manuscript received 23 May 2003; published 23 September 2003)

The method of moments is applied to an underdamped bistable oscillator driven by Gaussian white noise and a weak periodic force for the observations of stochastic resonance and the resulting resonant structures are compared with those from Langevin simulation. The physical mechanisms of the stochastic resonance are explained based on the evolution of the intrawell frequency peak and the above-barrier frequency peak via the noise intensity and the fluctuation-dissipation theorem, and the three possible sources of stochastic resonance in the system are confirmed. Additionally, with the noise intensity fixed, the stochastic resonant structures are also observed by adjusting the nonlinear parameter.

DOI: 10.1103/PhysRevE.68.036123 PACS number(s): 05.10.Gg, 05.40.−a, 05.20.−y, 85.30.De

I. INTRODUCTION

The conventional stochastic resonance (SR) is referred to as a synchronization phenomenon in an overdamped bistable system between the noise-induced transition and the external weak signal [1–3]. As the research on SR carried on in various directions, many interesting and meaningful results have been obtained nearly in every field, especially in the fields of neural information transmission [4–9] and signal processing [10–13], etc. Most of the results in these systems follow the conventional SR mechanism, whether the two stable attractors are static or dynamic.

Additionally, there exists a new type of SR in the underdamped monostable system [13,14], due to the approximate coincidence between the lowest-energy eigenfrequency and the drive frequency, which has been pointed out as a general phenomenon in all underdamped nonlinear oscillators. Alfonsi *et al.* [15] named this new type of SR intrawell SR, while they called the conventional SR interwell SR, realized numerically the double stochastic resonant structure in an underdamped bistable oscillator by investigating the evolution of the spectral amplitude at the driven frequency via the noise intensity, and concluded that both stochastic resonances coexist only when the forcing frequency takes values within a narrow range around the unperturbed characteristic frequency at the bottom of the wells. Since the fluctuating underdamped bistable oscillator has many applications such as in laser generation, passive optical transmission or forced oscillation of an electron in a Penning trap, and so on [16], the stochastic resonant behavior of this underdamped bistable oscillator will be investigated further from the viewpoint of linear response in this review.

Since the direct simulation about stochastic systems is always time consuming, there have been several theoretic techniques developed in the research on SR, such as linear response theory [2,16], adiabatic approximation [17], eigenfunction expansion [18], etc. Among these the linear response theory has been proven to be a powerful tool, based on which some approximate methods have been proposed, such as the matrix continuous fraction method [19] and the method of moments [20,21], etc. As far as the method of moments is concerned, Dykman *et al.* [20] first used it to investigate the effect of fluctuations on resonance nonlinear response of an underdamped monostable oscillator. Then Evstigneev *et al.* [21] presented a modified moment method to calculate the linear and nonlinear susceptibilities of an ensemble of biased overdamped oscillator and got novel resonant phenomena. Since the method of moments is a simple and convenient tool, our concern is what will occur if the modified method is applied in observing the SR in the underdamped bistable oscillator. To our knowledge, there have been a few studies (see Refs. [22,23]) on the SR in this system at the theoretic level, but they are based on adiabatic approximation, which requires the slowly varying periodic force (i.e., the drive frequency $\Omega \ll 1$) and weak noise intensity. In addition, the theoretic results in Refs. [22,23] only considered the interwell relaxation dynamics, so only the conventional SR was disclosed. But the dynamic characteristic of the system is more complex than the interwell relaxation dynamic, so using the method of moments we expect to disclose more general resonant results, which might be useful in the preceding applications or in signal processing.

The paper is organized as follows. In Sec. II, the method of moments for linear susceptibility is introduced. In Sec. III, the spectral amplification factors are calculated both from the method of moments and from Langevin equation simulation, so that the resonant structures derived from the two methods are compared and the applicability of the method of moments is analyzed. In Sec. IV, the dependence of the intrawell frequency peak and the above-barrier frequency peak on the noise intensity is investigated, and the physical mechanisms of the resonant structure are analyzed based on the fluctuation-dissipation theorem. In Sec. V, the SR induced by the nonlinear parameter is presented. In Sec. VI, the conclusions are drawn.

*Email address: kangyanmei2002@yahoo.com.cn
†Corresponding author. Email address: jxxu@mail.xjtu.edu.cn
‡Email address: xie813@263.net

II. THE METHOD OF MOMENTS FOR LINEAR SUSCEPTIBILITY

We consider the driven underdamped bistable oscillator modeled by the following Langevin equation:

$$\ddot{x}+\gamma\dot{x}-ax+bx^3=\epsilon(t)+\xi(t), \tag{1}$$

where $\epsilon(t)$ is a weak periodic force, $a>0$ and $b>0$ are parameters such that the system is bistable, $\gamma>0$ is the damping coefficient, and $\xi(t)$ is Gaussian white noise with correlation function $\langle\xi(t+\tau)\xi(t)\rangle=2D\gamma\delta(\tau)$. Here $\delta(\cdot)$ is the Dirac function and D is the noise intensity.

Let $p(x,y,t)$ denote the phase probability density of system (1) at time t with $y=\dot{x}$, and then the Fokker-Planck equation for the phase probability density is

$$\frac{\partial p}{\partial t}=D\gamma\frac{\partial^2 p}{\partial y^2}-\frac{\partial(yp)}{\partial x}+\frac{\partial\{[\gamma y-ax+bx^3-\epsilon(t)]p\}}{\partial y} \tag{2}$$

with $p(x,y,t)$ obeying natural boundary conditions at $x\to\pm\infty$ or $y\to\pm\infty$.

Let $G(x,y)$ be an arbitrary function of coordinates x and y, and suppose that the corresponding time-dependent moment of the coordinates

$$\langle G\rangle=\langle G(x,y)\rangle=\underbrace{\int\int}_{R^2}G(x,y)p(x,y,t)dxdy \tag{3}$$

exists. Then by multiplying the two sides of Eq. (2) with $G(x,y)$ and integrating it by means of the partial integration formula and the natural boundary conditions, we obtain the evolution equation for the moment $\langle G\rangle$,

$$\frac{d\langle G\rangle}{dt}=D\gamma\left\langle\frac{\partial^2 G}{\partial y^2}\right\rangle+\left\langle y\frac{\partial G}{\partial x}\right\rangle-\left\langle[\gamma y-ax+bx^3-\epsilon(t)]\frac{\partial G}{\partial y}\right\rangle. \tag{4}$$

For the sake of calculating susceptibility, we take $\epsilon(t)=\varepsilon e^{-i\Omega t}$ into account. According to Floquet's theory [3], the asymptotic solution of Eq. (2) is time periodic and has the same period as the external force. We assume $\varepsilon\ll 1$ and seek the asymptotic probability in linear response background [20,21,24] as

$$p_{as}(x,y,t)=p_0(x,y)+p_1(x,y)\varepsilon e^{-i\Omega t}, \tag{5}$$

where $p_0(x,y)$ is the stationary probability density of system (1) in the case of $\epsilon(t)=0$. It is well known that

$$p_0(x,y)=Z^{-1}e^{\{-(1/D)[1/2y^2-(a/2)x^2+(b/4)x^4]\}}, \tag{6}$$

where Z is a normalization constant. It can be easily induced from the normalization property of the probability $p(x,y,t)$ that

$$\underbrace{\int\int}_{R^2}p_1(x,y)dxdy=0. \tag{7}$$

With formula (5) substituted into formula (3) and Eq. (4), respectively, and using the orthogonality of trigonometric functions, we derive the following:

$$\langle G\rangle_{as}=\langle G\rangle_0+\langle G\rangle_1\varepsilon e^{-i\Omega t}, \tag{8}$$

$$D\gamma\left\langle\frac{\partial^2 G}{\partial y^2}\right\rangle_0+\left\langle y\frac{\partial G}{\partial x}\right\rangle_0-\left\langle(\gamma y-ax+bx^3)\frac{\partial G}{\partial y}\right\rangle_0=0, \tag{9}$$

$$-i\Omega\langle G\rangle_1=D\gamma\left\langle\frac{\partial^2 G}{\partial y^2}\right\rangle_1+\left\langle y\frac{\partial G}{\partial x}\right\rangle_1-\left\langle(\gamma y-ax+bx^3)\frac{\partial G}{\partial y}\right\rangle_1+\left\langle\frac{\partial G}{\partial y}\right\rangle_0 \tag{10}$$

with

$$\langle G\rangle_{as}=\underbrace{\int\int}_{R^2}G(x,y)p_{as}(x,y,t)dxdy$$

and

$$\langle G\rangle_{0,1}=\underbrace{\int\int}_{R^2}G(x,y)p_{0,1}(x,y)dxdy.$$

Since every continuous function can be approximated by the sum of polynomials, with the boundary conditions taken into account we let

$$p_1(x,y)=p_0(x,y)\sum_{k=0}^{\infty}\sum_{j=0}^{k}c_{k,j}x^j y^{k-j}, \tag{11}$$

where coefficients $c_{k,j}$ are unknown. Substitution of $G(x,y)$ with the ordinary moment functions

$$G(x,y)=x^m y^l, m,l=0,1,2,\ldots \tag{12}$$

and insertion of expansion (11) into formula (7) and Eq. (10) yield a infinite-dimensional linear algebraic system for $c_{k,j}$ as follows:

$$\sum_{k=0}^{\infty}\sum_{j=0}^{k}c_{k,j}\langle x^j y^{k-j}\rangle_0=0,$$

$$\sum_{k=1}^{\infty}\sum_{j=0}^{k}\{m\langle x^{m+j-1}y^{k-j+l+1}\rangle_0 - l(\gamma\langle x^{m+j}y^{k-j+l}\rangle_0 - a\langle x^{m+j+1}y^{k-j+l-1}\rangle_0 + b\langle x^{m+j+3}y^{k-j+l-1}\rangle_0) + D\gamma l(l-1)\langle x^{m+j}y^{k-j+l-2}\rangle_0 + i\Omega(\langle x^{m+j}y^{k-j+l}\rangle_0 - \langle x^j y^{k-j}\rangle_0\langle x^m y^l\rangle_0)\}c_{k,j} = -l\langle x^m y^{l-1}\rangle_0 \quad (13)$$

with $m,l=0,1,2,\ldots$.

In order to solve this linear system (13), we must make a truncation on k. We take

$$p_1(x,y)\approx p_0(x,y)\sum_{k=0}^{N}\sum_{j=0}^{k}c_{k,j}x^j y^{k-j} \quad (14)$$

and m and l satisfying $(m+l)\leqslant N$ into account, then the infinite-dimensional system changes into a finite-dimensional linear algebraic system. The truncated linear system is solved numerically using LSARG where the concerned stationary moments $\langle\cdot\rangle_0$ are estimated by the routine QDAGI of MS-IMSL math function library.

Since $\varepsilon\ll 1$ is supposed, by the linear response theory the quantity

$$\chi(\Omega)=\underbrace{\int\int}_{R^2}xp_1(x,y)dxdy \quad (15)$$

is the linear susceptibility, which describes the long time ensemble-averaged response of system (1) to a weak force of frequency $f_d=\Omega/2\pi$ in the sense of the first-order harmonic [20,21,24,25]. If we take $\epsilon(t)=\varepsilon\cos(\Omega t)$ into account, then from formulas (8) and (15) and the relation $\chi(-\Omega)=\overline{\chi(\Omega)}$ (the overline represents conjugate operation) the response approximately reads $\langle x(t)\rangle_{as}=\varepsilon|\chi(\Omega)|\cos(\Omega t+\phi)$ with $\phi=-\arctan[\mathrm{Im}\,\chi(\Omega)/\mathrm{Re}\,\chi(\Omega)]$. Here Re $\chi(\Omega)$ and Im $\chi(\Omega)$ represent the real part and the imaginary part of $\chi(\Omega)$, respectively. Another quantity $|\chi(\Omega)|^2$, the spectral amplification factor for the first order harmonic, is often used as a measurement for the stochastic resonant behavior. With the method of moments, we calculate the spectral amplification factor from formulas (14) and (15).

III. SPECTRAL AMPLIFICATION FACTOR AND THE APPLICABILITY OF THE METHOD OF MOMENTS

Since the susceptibility from the method of moments is related to N, the order for truncation, the accuracy of the calculated spectral amplification factor is also affected by N. If numerical error is not of concern, the larger N is, the more accurate the results are. However, when N is large to an extent, the coefficient matrix of the linear algebraic systems is ill-conditioned, which makes the efficiency of a linear solver become important, and certain methods, such as the Gaussian elimiation procedure, are found to be inefficient.

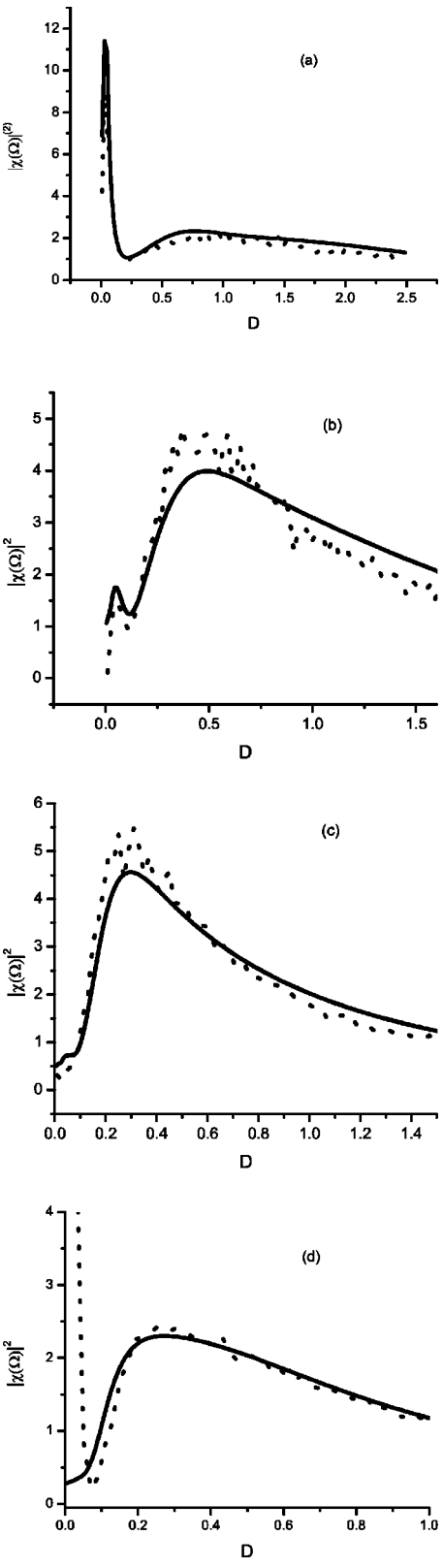

FIG. 1. The spectral amplification factor via the noise intensity: the method of moments (solid) and Langevin simulation (dot). The parameters $a=1.0$, $b=1.0$, $\gamma=0.1$ and f_d is (a) 0.2, (b) 0.16, (c) 0.12, (d) 0.05.

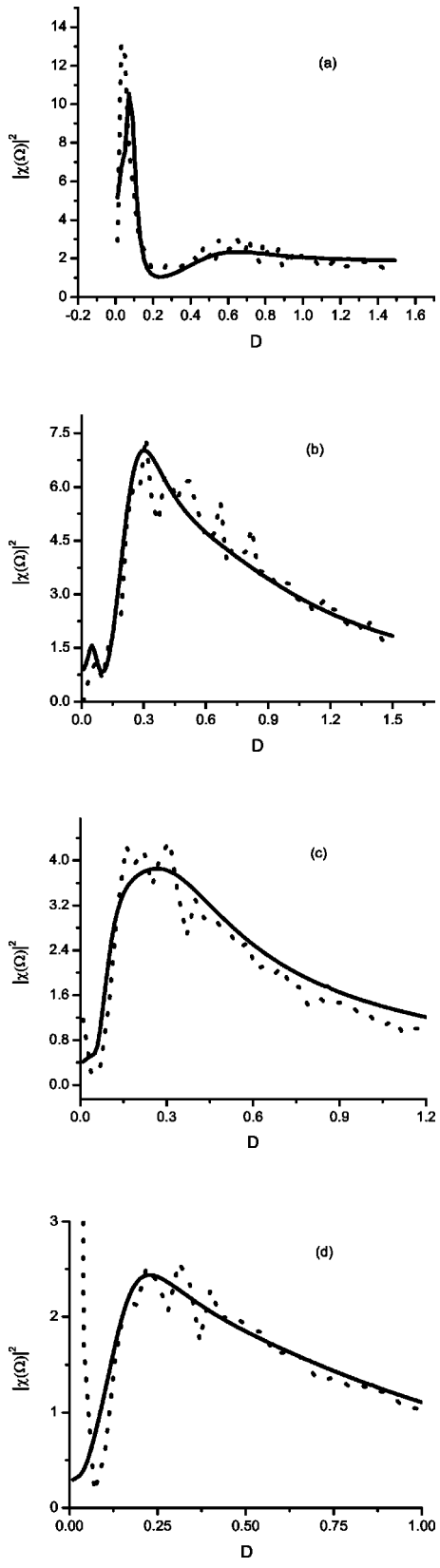

FIG. 2. The spectral amplification factor via the noise intensity: the method of moments (solid) and Langevin simulation (dot). The parameters $a=1.0$, $b=1.0$, $\gamma=0.05$ and f_d is (a) 0.19, (b) 0.15, (c) 0.1, (d) 0.05.

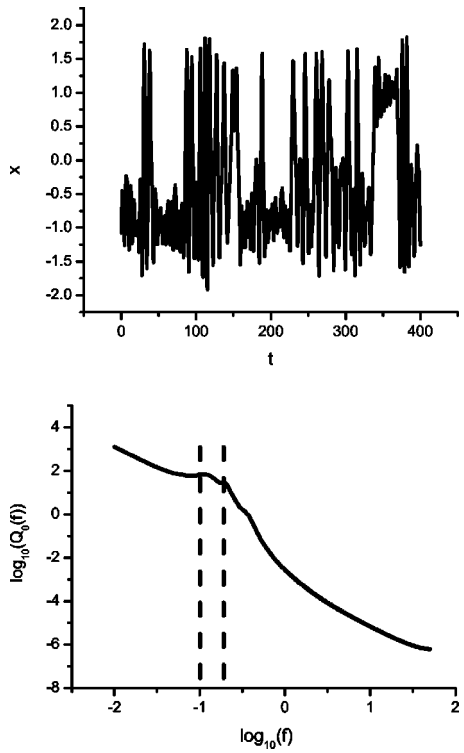

FIG. 3. A time series of coordinates consists of three types of motions (up) and the SDF (down) with $a=1.0$, $b=1.0$, $\gamma=0.1$, and $D=0.13$. The vertical dashed lines mark the locations of the nonzero frequency SDF peaks, from the left to the right they are the overbarrier spectral peak and the intrawell vibration spectral peak.

Even with a more efficient linear solver, such as LSARG, the unbounded increase of N still results in a lack of smoothness in the resonant curves. Along with the poor condition of the system, the rounding error in the concerned higher-order moments $\langle\ \rangle_0$ might be a cause. By observing the spectral amplification factor via the noise intensity, we see that although all stochastic resonant peaks have appeared in the case of $N=3$ for larger damping coefficient, such as $\gamma=0.1$, their heights or locations have evident variations up to $N=11$. We also observe that for a smaller damping coefficient, such as $\gamma=0.05$, the convergence of the resonant curves can be observed only when N is much larger, for example, $N=23$. Below we present the dependence of the spectral amplifica-

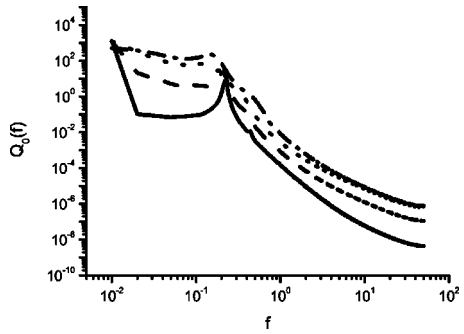

FIG. 4. The SDF with parameters $a=1.0$, $b=1.0$, $\gamma=0.1$, and D is 0.01 (solid), 0.05 (dashed), 0.15 (dotted), 0.5 (dash-dotted).

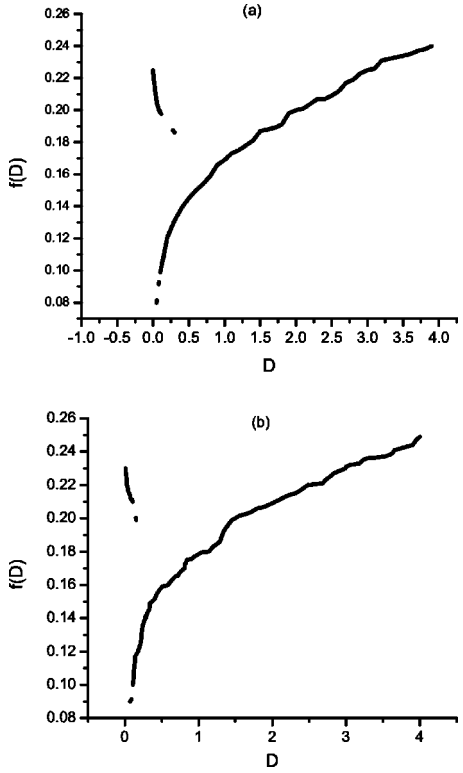

FIG. 5. The peak frequencies vs noise intensity with parameters $a=1.0$, $b=1.0$, $\epsilon(t)=0$ and γ is (a) 0.1, (b) 0.05. The upper branches represent the intrawell frequency peak, the lower represent the overbarrier frequency peak, and the solid curves show the peak frequency with larger spectral amplitude.

tion factor on the noise intensity with $N=13$ in Fig. 1 and $N=19$ in Fig. 2, respectively.

To check the accuracy of the method of moments, we compare the results of the method of moments with those of Langevin simulation of system (1). On the basis of the linear response theory, the susceptibility $\chi(\Omega)$ can also be found in terms of the fluctuation-dissipation theorem (FDT) [13,20,25]

$$\mathrm{Re}\ \chi(\Omega)=\frac{2}{D}P\int_0^{+\infty}d\omega\,\frac{\omega^2 Q_0(\omega)}{\omega^2-\Omega^2}, \tag{16}$$

$$\mathrm{Im}\ \chi(\Omega)=\frac{\pi\Omega}{D}Q_0(\Omega). \tag{17}$$

Here $Q_0(\omega)$ is the spectral density of fluctuations (SDF) of the coordinates x of the system in the absence of the periodic force and P implies the Cauchy principal part. In the simulation, we use Runge-Kutta fourth-order routine and Box-Mueller algorithm [26] to integrate Eq. (1) in the absence of the periodic force using the steplength $\triangle t=0.005$. We take 10 000 data points in one sample with the sample frequency $f_s=100$ Hz and apply Welch's periodogram method to 500–1000 such samples to get the SDF. Then we use the Hilbert transform to calculate integration (16). The results (with a scale acted on) of Langevin simulation are also plotted in Figs. 1 and 2.

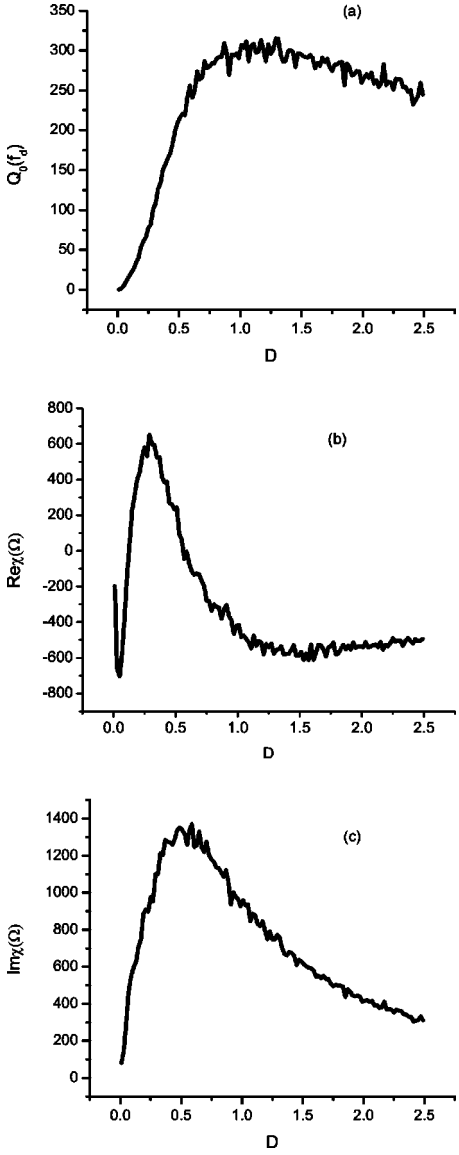

FIG. 6. Langevin simulation results in terms of the FDT for the parameters $a=1.0$, $b=1.0$, $\gamma=0.1$, $\varepsilon=0.0$, and $f_d=0.16$. (a) The spectral amplitude of the SDF at the drive frequency via the noise intensity; (b) the real part of the susceptibility via the noise intensity; (c) the imaginary part of the susceptibility via the noise intensity.

From Figs. 1(b)–1(c) and Figs. 2(a)–2(d) we can see that the resonant structures of the method of moments and those of Langevin simulation not only have the same number of the resonant peaks, but have almost the same peak locations for given parameters. But for γ in zero limit (the plots are omitted), we see that although the resonant curves from the method of moments (when $N=21$) exhibit almost the same shapes as the curves from Langevin simulation, the former has not attained its convergence, and with N further increased, numeric rounding error can induce redundant peaks in the resonant structure.

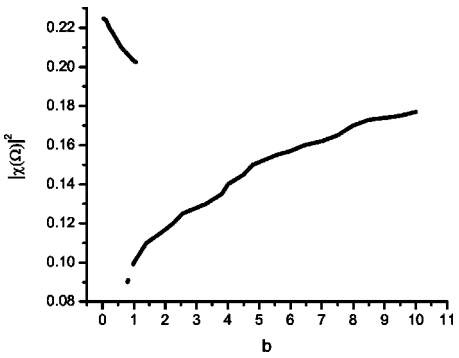

FIG. 7. The peak frequencies vs nonlinear coefficient with $a=1.0$, $\gamma=0.1$, $\epsilon=0.0$, and $D=0.1$. The upper branch represents the intrawell frequency peak, the lower represents the overbarrier frequency peak, and the solid curve shows the peak frequency with larger spectral amplitude.

IV. THE PHYSICAL MECHANISMS OF THE RESONANT STRUCTURE

The curves in Figs. 1 and 2 show us that for certain drive frequencies, there might exist double resonant peaks at different noise intensity. What we want to know exactly is for which drive frequencies and why a double resonant structure occurs. In the SDF of the underdamped monostable oscillator, there is a sharp spectral peak riding over the smooth Lorenz spectrum of the background noise. Lindner *et al.* called the frequency where the maximum spectral amplitude is observed as the natural frequency peak, and disclosed that the response of the underdamped monostable oscillator is maximized when the natural frequency peak is shifted to the drive frequency by the noise [27,28]. Compared with the underdamped monostable oscillator, the SDF of the underdamped bistable oscillator has a more complex structure. The existence of bistability of the potential energy results in three different types of motions and thus there are three distinct peaks in the distribution of the SDF within a certain parameter range [29–31], as shown in Figs. 3 and 4. The zero-frequency peak is due to jumps between wells, the peak close to the unperturbed eigenfrequency at the bottom of the wells is due to vibrations near the well bottom, and the middle peak is due to the vibrations over the barrier. Below we refer to the two frequencies where the two nonzero-frequency spectral peaks are observed as the intrawell frequency peak and the above-barrier frequency peak, respectively. The dependence of the intrawell frequency peak and the above-barrier frequency peak on the noise intensity is shown in Fig. 5. The figures show us that as the noise intensity increases, the intrawell frequency peak descends from unperturbed characteristic frequency at the bottom of the wells till disappearance, while the above-barrier frequency peak continuously ascends from a value larger that zero. Moreover, the solid curves tell us that the intrawell vibration dominates when the noise intensity is lower, and the above-barrier vibration overwhelms it when the noise intensity becomes larger and the system response becomes more like that of the underdamped monostable oscillator. Since the intrawell frequency peak and the above-barrier frequency peak, just as the natural frequency peak, are noise tunable, we infer that

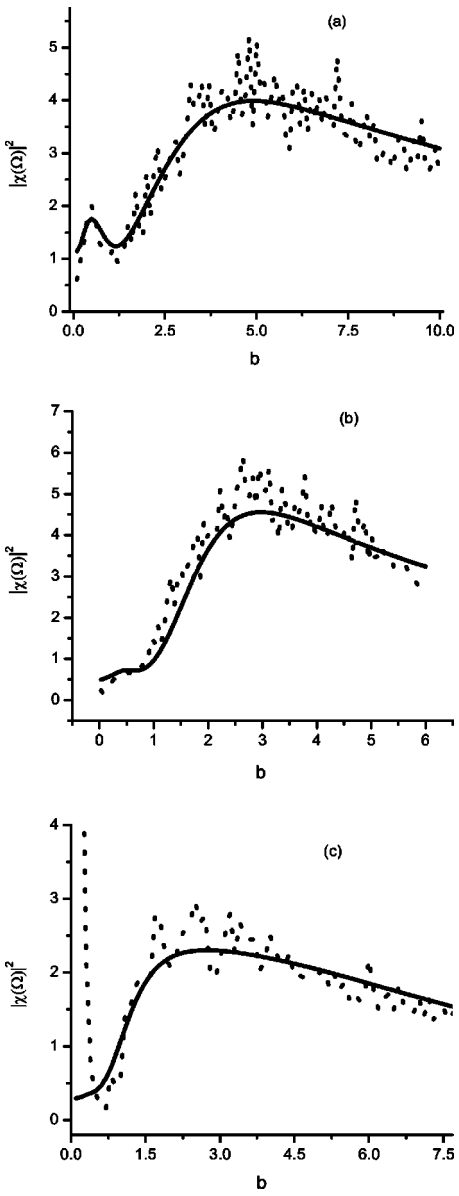

FIG. 8. Spectral amplification factor vs nonlinear coefficient by the method of moments (solid) and Langevin simulation (dot). The parameters $a=1.0$, $\gamma=0.1$, and $D=0.1$ and f_d is (a) 0.16, (b) 0.12, (c) 0.05.

the evolution of the two nonzero-frequency spectral peaks via the noise intensity is important for the understanding the nonconventional SR in the system under consideration.

Now let us turn to the FDT. If the two branches of Fig. 5 cross the drive frequency twice, then $Q_0(\Omega)$ as a function of D has two maxima, and then the quantity Im $\chi(\Omega)$ has two sharp peaks at the noise intensities a little less than the noise intensities where $Q_0(\Omega)$ attains its maxima; while from simulations we know the quantity Re $\chi(\Omega)$ successively passes a minimum and a maximum at noise intensities less than the noise intensities where Im $\chi(\Omega)$ takes its maxima. But in this case, $|\chi(\Omega)|^2$ has the shape of $Q_0(\Omega)$ with nearly the peak locations. Therefore, we see that the nonconventional double structure can occur in the system when the intrawell frequency peak and the above-barrier frequency

peak are shifted to the drive frequency twice, as seen from Figs. 1 and 2(a). However, from Figs. 1 and 2(b), we see that even if only the above-barrier frequency peak is shifted to the drive frequency, double resonant structure might still be observed. The occurrence of the second peak in Figs. 1 and 2(b), as the single peak in Figs. 1 and 2(c), is due to the overbarrier vibration, but the occurrence of the first peak needs special remark. From Fig. 6, we see that although the quantity $Q_0(\Omega)$ or Im $\chi(\Omega)$) is monopeak, Re $\chi(\Omega)$ has a minimum when the noise is weak and it is the minumum that make the major contribution to the first resonant peak in Fig. 1(b). With the analysis of formula (16) and the structure of SDF for different noise intensity we infer that the first peak is a result of the occurrence of the overbarrier vibration in low-frequency band when the noise is weak, which again results from the noise-induced slowing down of the intrawell vibration near the top of the barrier [31]. Therefore, for the drive frequency that ranges from the least overbarrier frequency peak to the unperturbed characteristic frequency at the bottom of the wells, one can expect a double resonant structure with the first resonant peak becoming more prominent as the drive frequency more approximates the unperturbed characteristic frequency at the bottom of the wells. This is consistent with the conclusion in Ref. [15]. Moreover, from the above analyses, we see the double resonant peaks are both associated with the intrawell or the overbarrier vibrations, so they both are nonconventional SR. But the above-barrier vibration was taken for the interwell jump in [15], so that the second resonant peak associated with it was thought of as the conventional SR behavior. In fact, the conventional SR behavior is due to the interwell jump, whose relaxation time can be tuned to match the drive frequency [22,23] as for standard overdamped systems, and the conventional SR is connected with the zero-frequency spectral peak of the system [13], as plotted in Figs. 1 and 2(d). Therefore, there are three sources of SR in the system and our analysis confirms this.

V. SR INDUCED BY PARAMETER

Since the structure of the SDF of system (1) is related with its potential shape, we can shift the intrawell frequency peak and the above-barrier frequency peak by adjusting the system parameter, for example, by changing the nonlinear coefficient. With the noise intensity fixed, the dependence of the two nonzero frequency peaks on the nonlinear coefficient is plotted in Fig. 7. Obviously, the behavior of two frequency peaks in this case is similar to that in Figs. 5(a) and 5(b). So the previously presented structures of SR can be observed again, as shown in Figs. 8(a)–8(c). It has been thought [12] that in the application of the phenomenon of SR to signal processing, the noise intensity is not always a tunable quantity; contrarily, the system parameters might be altered. Thus, the SR induced by the nonlinear parameter might have importance in signal processing. Additionally, with the other parameters fixed, the increase of the damping coefficient weakens both the intrawell vibration and the overbarrier vibration, so that the nonconventional double resonant peak induced by the damping coefficient cannot occur. The further results are omitted here.

VI. CONCLUSIONS

In order to demonstrate the accuracy of the method of moments for the observation of SR in the periodically driven stochastic underdamped bistable oscillator, the spectral amplification factor is calculated both from the method of moments and from Langevin simulation. When the damping coefficient is not in zero limit, good agreement is found between the results obtained using the two methods.

Based the dependence of the intrawell frequency peak and the above-barrier frequency peak of the SDF of the system on the noise intensity and the FDT, the three sources of the SR in the system are confirmed and the physical mechanism of the double resonant structures is analyzed. With the noise intensity fixed, the SR induced by the nonlinear parameter is also observed. The resonant structure when the damping coefficient is in zero limit will be studied in the future.

ACKNOWLEDGMENTS

This work was supported by the National Science Foundation with Grant Nos. 19972051, 10172067, and 30030040. Yan-Mei Kang thanks Barbara J. Breen, John F. Lindner, and M. Evstigneev for helpful suggestions.

[1] L. Gammaitoni *et al.*, Rev. Mod. Phys. **70**, 223 (1998).
[2] M.I. Dykman *et al.*, Nuovo Cimento **17D**, 661 (1995).
[3] P. Hung, Phys. Rep. **234**, 175 (1993).
[4] J.P. Segundo *et al.*, in *Origins: Brain and Self Organization*, edited by K.H. Pribram (Lawrence Erlbaum Associates, Hillsdale, New Jersey, 1994), pp. 300–311.
[5] J. Douglass *et al.*, Nature (London) **365**, 337 (1993).
[6] A. Longtin, J. Stat. Phys. **70**, 309 (1993).
[7] Y.F. Gong *et al.*, Phys. Lett. A **243**, 351 (1998).
[8] P.L. Gong and J.X. Xu, Phys. Rev. E **63**, 031906 (2001).
[9] P.L. Gong, J.X. Xu, and S.J. Hu, Chaos, Solitons Fractals **13**, 885 (2002).
[10] G. Hu *et al.*, Chin. Phys. Lett. **9**, 69 (1992).
[11] S. Mitaim and B. Kosko, Proc. IEEE **86**, 2152 (1998).
[12] B.H. Xu *et al.*, Chaos, Solitons Fractals **13**, 633 (2002).
[13] N.G. Stocks, N.D. Stein, and P.V.E. McClintock, J. Phys. A **26**, L385 (1993).
[14] M.I. Dykman *et al.*, J. Stat. Phys. **70**, 479 (1993).
[15] L. Alfonsi *et al.*, Phys. Rev. E **62**, 299 (2000).
[16] M.I. Dykman and P.V.E. McClintock, Physica D **58**, 10 (1992).
[17] B. McNamara and K. Wiesenfeld, Phys. Rev. A **39**, 4854 (1989).
[18] G. Hu, G. Nicolis, and C. Nicolis, Phys. Rev. A **42**, 2030 (1990).
[19] P. Jung, Z. Phys. B: Condens. Matter **76**, 521 (1989).
[20] M.I. Dykman *et al.*, Phys. Rev. E **54**, 2366 (1996).
[21] M. Evstigneev, V. Pankov, and R.H. Prince, J. Phys. A **34**, 2595 (2001).

[22] L. Gammaitoni *et al.*, Phys. Rev. A **40**, 2114 (1989).
[23] Y.M. Kang, J.X. Xu, and Y. Xie, Acta Phys. Sin. **52**, 802 (2003).
[24] H. Risken, *The Fokker-Planck Equation* (Springer-Verlag, Berlin, 1984).
[25] N.G. Stocks *et al.*, in *Fluctuations and Order: The New Synthesis*, edited by M. Millonas (Springer, Berlin, 1996), pp. 53–68.
[26] R.F. Fox, I.R. Gatland, G. Vemuri, and R. Roy, Phys. Rev. A **38**, 5938 (1988).
[27] J.F. Lindner *et al.*, Phys. Rev. E **63**, 051107 (2001).
[28] J.F. Lindner *et al.*, Phys. Rev. E **66**, 013102 (2002).
[29] K. Voigtlaender and H. Risken, J. Stat. Phys. **40**, 397 (1985).
[30] M.I. Dykman, S.M. Soskin, and M.A. Krivoglaz, Physica A **133A**, 53 (1985).
[31] M.I. Dykman *et al.*, Phys. Rev. A **37**, 1303 (1988).